Moving Ion Fronts in Mixed Ionic-Electronic Conducting Polymer Films

Sarah E. Feicht, George D. Degen, and Aditya S. Khair
Dept. of Chemical Engineering, Carnegie Mellon University, Pittsburgh, PA 15213

DOI 10.1002/aic.14746
Published online February 8, 2015 in Wiley Online Library (wileyonlinelibrary.com)

The aim of this paper is to analyze moving front dynamics of ions and holes in a planar, mixed ionic-electronic conducting polymer film. As cations invade the film, holes evacuate; thus, an ionic current is converted to an electronic signal. Recent experiments show that the location of the advancing ion front increases as the square-root of time, a scaling typically associated with diffusive transport, which is surprising given the large driving voltages utilized. Ionic and electronic transport is modeled via the drift-diffusion equations. A similarity transformation reduces the governing partial differential equations to ordinary differential equations that are solved numerically. The similarity transformation elucidates the origin of the square-root-of-time front scaling. The similarity solution is then compared to the numerical solution of the full drift-diffusion equations, finding excellent agreement. When compared with experimental data, our model captures the front location; however, qualitative differences between the ion profiles are observed. © 2015 American Institute of Chemical Engineers *AIChE J*, 61: 1447–1454, 2015
Keywords: mixed ionic-electronic conductor, organic electronics, similarity solution, drift-diffusion equations, charge transport

Introduction

Mixed ionic-electronic conductors (MIECs) are materials that conduct both electronic (electrons or holes) and ionic charge carriers.[1] Certain organic semiconductors are MIECs; the ability to transport ionic and electronic charge carriers opens up organic electronics to a wide range of promising applications including gas sensors,[2,3] light-emitting electrochemical cells,[4,5] superconductors,[6,7] and transistors.[8,9]

MIECs based on organic semiconductors are used in biosensors to detect the presence of ions in biological tissue.[10] An example biosensor device is the organic electrochemical transistor[11] (OECT), which consists of a gate electrode immersed in an electrolyte, in contact with an organic semiconductor film sandwiched between a grounded source electrode and a drain electrode where the voltage is applied.[12] The applied voltage drives the injection of ions from the electrolyte into the polymer film. The ions displace electronic charge carriers that evacuate the thin film across the source electrode, resulting in the conversion of an ionic current to an electrical signal. For example, Bernards et al.[13] used an OECT to measure glucose concentrations in the blood stream, while Tarabella et al.[14] designed an OECT to monitor micelle formation in an electrolyte. The conjugated polymer poly(3,4-ethylenedioxythiophene) doped with negatively charged poly(styrenesulfonate) (PEDOT:PSS) is an organic biocompatible MIEC commonly used in biosensors due to its high ion and hole mobilities, flexibility, and stability.[15]

The electrical mobility is defined as the ratio of the drift velocity of a charged species to the magnitude of the applied electric field.[16] Accurate prediction and measurement of the mobility of ionic species in an organic MIEC is a key to characterizing ion transport. However, the mobility is challenging to determine because standard techniques to measure charge carrier mobility, such as time of flight measurements,[17] are difficult to implement in organic MIECs.[18] Stavrinidou et al.[18] designed a device to measure ion mobility in organic MIECs, which is depicted in Figure 1. Their device is comprised of a gold cathode adjacent to a PEDOT:PSS polymer thin film in contact with an electrolyte. A reference electrode in the electrolyte completes the circuit. The polymer thin film is enriched in holes compensated by the fixed negative charge on the functional groups of PSS. When a constant voltage is applied across the electrodes, the cations displace the positively charged holes, which exit at the cathode resulting in an electric signal indicating the presence of invading ions. The PEDOT:PSS is electrochromic, so the film changes color based on the density of electrons and holes. As the holes evacuate, transmittance of light through the device increases. The measured change in transmittance ΔT is the change in transmittance relative to the transmittance in the absence of an applied field. Stavrinidou et al.[18] measured the transmittance along the film with time to determine the profile of the invading cations. They define the cation drift length δ as the location where ΔT is one half of its maximum value. Stavrinidou et al.[18] find that the drift length increases as the square-root of time, $\delta \sim t^{1/2}$, for a

This contribution was identified by Norman Loney (New Jersey Institute of Technology) as the Best Paper in the session "Mathematical Modeling of Transport Processes" of the 2013 AIChE Annual Meeting in San Francisco, CA.

Correspondence concerning this article should be addressed to S. E. Feicht at sfeicht@cmu.edu.

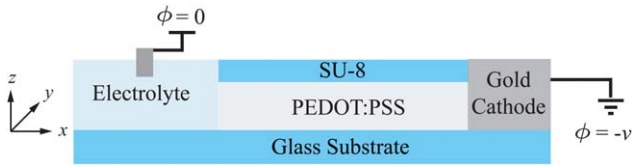

Figure 1. Schematic of the planar organic semiconductor device designed by Stavrinidou et al.[18]

The device consists of a 32 mm × 16 mm × 400 nm (*x*×*y*×*z*) PEDOT:PSS film in contact with a gold cathode and an electrolyte reservoir, sandwiched between an SU-8 ion barrier layer and a glass substrate. The potential is ϕ. The magnitude of the applied voltage, *v*, is around 2 volts. [Color figure can be viewed in the online issue, which is available at wileyonlinelibrary.com.]

range of electrolytes. Thus, it is inferred that the moving cation front also advances as $t^{1/2}$.

In an earlier article, Stavrinidou et al.[19] analyzed the invasion of cations via a circuit model comprised of two resistors in series. The holes are far more mobile than the ions, hence the voltage drops primarily across the cation-rich region, or resistor. They found that the drift length $\delta = \sqrt{2\mu_p v t}$ where μ_p is the cation mobility and v is the applied voltage. Stavrinidou et al.[18] combined this result with the measurement of the change in drift length with time to determine the cation mobility, μ_p, assumed to be a constant (i.e., no field dependence). They also solved the governing differential equations for charge carrier transport numerically to confirm the $\delta = \sqrt{2\mu_p v t}$ relation.

The square-root-of-time front scaling is intriguing for several reasons. First, this scaling is typically associated with a diffusive process, yet in this case electromigration is expected to dominate ion transport due to the large applied voltage. We define "large" as an applied voltage much greater than the thermal voltage, $k_B T/q \approx 26$ mV, where k_B is the Boltzmann constant, T is temperature, and q is the charge of a proton. However, diffusion presumably plays a role as the measured and calculated cation density profiles are not sharp fronts, as would be expected if ion transport were solely due to electromigration. Moreover, the spatial cation profiles noticeably broaden in time due to diffusion. What is the relative importance of diffusion vs. migration? Additionally, the invading cations eventually reach the cathode, so the $\delta \sim t^{1/2}$ scaling cannot persist indefinitely. When does the scaling break down? Here, we answer these questions by constructing and analyzing a mathematical model for the front invasion dynamics.

Moving front dynamics of charged species also appear during redox reactions and electrical switching in conjugated polymer thin films,[20–23] and in electrophoretic separations in aqueous media.[24–27] The advancement of the moving front can be linear in time t[21,25,26] or proportional to $t^{1/2}$ [20,22,23,27] depending on the material properties and device geometry. Mani et al.[28] and Zangle et al.[29] demonstrated that ion concentration polarization fronts at a microchannel-nanochannel junction can propagate as enrichment and depletion shocks. Under a constant current, these shocks advance linearly in time; for a fixed potential difference, the shocks advance as $t^{1/2}$ and the shock thickness increases as $t^{1/2}$.[30] Mani and Bazant[31] demonstrated that a variety of scalings for the shock advancement and thickness can be obtained in microchannels with a power-law growth in width; moreover, the evolution of the shock is self-similar. It will be shown that the present problem shares certain similarities to the propagation of concentration polarization under constant voltage.

In the following section, we present the governing drift-diffusion equations for ion invasion across an MIEC film. Next, we simplify the drift-diffusion equations in the experimentally relevant limits of large applied voltage, a high hole mobility to cation mobility ratio, and local electroneutrality. We apply a similarity transformation to the simplified drift-diffusion equations governing the cation invasion and hole displacement. The results section includes comparisons between the similarity solutions and numerical solution of the full drift-diffusion equations. We then compare our results to the experiments of Stavrinidou et al.[18]

Governing Equations

The invasion of cations and displacement of holes in a planar MIEC device is depicted in Figure 2. Figure 2a shows the device at time $t = 0$ when the electric field is applied. Initially, the polymer film is enriched in holes compensated by fixed anions supplied by the polymer backbone. We assume that the initial hole and fixed anion densities are uniform. In Figure 2b, at a later time $t > 0$, cations are injected at the electrolyte-polymer interface and invade the film, displacing holes that evacuate across the cathode. The electrolyte is assumed to be a well-mixed reservoir. The cathode accepts holes but is a blocking electrode for the ions; similarly, holes do not enter the electrolyte reservoir. To model ionic and electronic charge transport in this device, we turn to the drift-diffusion equations, which consist of an equation for carrier flux that accounts for both diffusion and migration of charged species, a charge conservation equation, and Poisson's equation that relates the electric field to the local charge density. Note, the drift-diffusion equations are mathematically equivalent to the Poisson–Nernst–Planck equations: the former is typically used as a moniker for electronic charge transport, the later for ionic transport. Here, we refer to the governing equations for ionic and electronic transport as the drift-diffusion equations uniformly. Given the device dimensions, 32 mm × 16 mm × 400 nm ($x \times y \times z$),[18] we assume that the ion and hole transport is predominately one-dimensional (1-D) along the x-direction between the electrolyte and the electrode.

The flux of a charged species is equal to the sum of the fluxes due to diffusion and migration. The cation flux j_p is

$$j_p = -\mu_p \frac{k_B T}{q} \frac{\partial p}{\partial x} + \mu_p p e \tag{1}$$

where p is the cation density, $e = -\partial\phi/\partial x$ is the electric field, ϕ is the electric potential, and x is the position in the direction of the width of the thin film. Similarly, the flux of holes j_h is

$$j_h = -\mu_h \frac{k_B T}{q} \frac{\partial h}{\partial x} + \mu_h h e \tag{2}$$

where h is the hole density and μ_h is the hole mobility. The flux of mobile anions from the reservoir is

$$j_n = -\mu_n \frac{k_B T}{q} \frac{\partial n}{\partial x} - \mu_n n e \tag{3}$$

where n is the mobile anion density and μ_n is the anion mobility. Poisson's equation relates the variation in electric field to the local space charge density

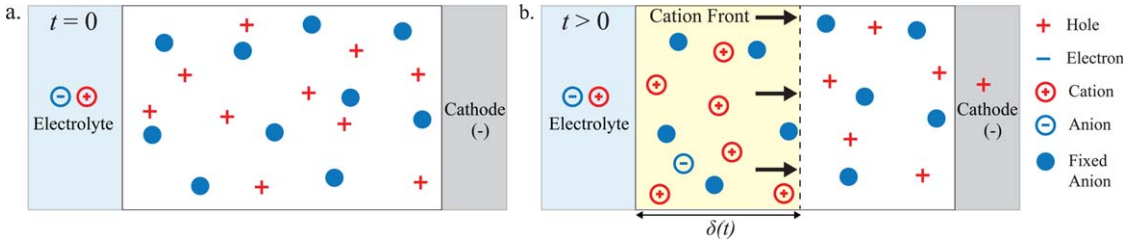

Figure 2. Cation invasion schematic: (a) initially, the thin film includes uniformly distributed fixed anions and holes. (b) After a potential is applied, cations (and some anions) enter the film, displacing holes.

The invasion length is $\delta(t)$. [Color figure can be viewed in the online issue, which is available at wileyonlinelibrary.com.]

$$\frac{\partial e}{\partial x}=\frac{q}{\varepsilon}(p+h-n-a) \tag{4}$$

where a is the density of the uniform, fixed anions on the polymer backbone and ε is the permittivity of the film. The final set of equations are charge conservation equations

$$\frac{\partial p}{\partial t}=-\frac{\partial j_p}{\partial x},\ \frac{\partial h}{\partial t}=-\frac{\partial j_h}{\partial x},\ \text{and}\ \frac{\partial n}{\partial t}=-\frac{\partial j_n}{\partial x} \tag{5}$$

where t is time.

At the electrolyte-polymer film interface, we assume that the reservoir concentration of ions is equal to the concentration of fixed anions on the polymer backbone. At the electrode, we assume that there are no faradaic reactions between the ions and the electrode, regardless of the applied voltage. This assumption is dependent on the ion and electrode material selected. The corresponding boundary condition is a no-flux condition for the ions. Initially, the cation density in the film is zero. The boundary and initial conditions for cations are expressed mathematically as

$$p(0,t)=a,\ \frac{k_BT}{q}\frac{\partial p(l,t)}{\partial x}=p(l,t)e(l,t),\ \text{and}\ p(x,0)=0 \tag{6}$$

where l is the width of the polymer film. Similarly, the boundary and initial conditions for anions are

$$n(0,t)=a,\ \frac{k_BT}{q}\frac{\partial n(l,t)}{\partial x}=-n(l,t)e(l,t),\ \text{and}\ n(x,0)=0 \tag{7}$$

The boundary conditions for the holes include a no-flux condition at the electrolyte-polymer interface, because the electrolyte does not conduct holes, and a reservoir condition at the electrode. Initially, the hole density is assumed to be equal to the fixed anion density. These conditions are

$$\frac{k_BT}{q}\frac{\partial h(0,t)}{\partial x}=h(0,t)e(0,t),\ h(l,t)=a,\ \text{and}\ h(x,0)=a \tag{8}$$

The boundary conditions for the electric potential are

$$\phi(0,t)=0\ \text{and}\ \phi(l,t)=-v \tag{9}$$

corresponding to a fixed potential difference v across the film.

We now nondimensionalize the governing equations by normalizing p, n, and h by a, the uniform negative backbone density; x by l, the width of the thin film; and e by v/l, the applied voltage divided by the width of the film. Time t is normalized by the time for cations to migrate across the film at a given applied voltage, $t\sim l^2/\mu_p v$. There is evidence that the carrier mobility is field-dependent in disordered polymers,[32,33] however, for simplicity, we assume that all carrier mobilities are constant.

The dimensionless charge conservation equations for cations and anions (5), when the equations for flux (1)–(3) are inserted, are

$$\frac{\partial\hat{p}}{\partial\hat{t}}=\frac{1}{\hat{v}}\frac{\partial^2\hat{p}}{\partial\hat{x}^2}-\frac{\partial}{\partial\hat{x}}(\hat{p}\hat{e})\ \text{and}\ \frac{\partial\hat{n}}{\partial\hat{t}}=\frac{1}{\hat{v}}\frac{\partial^2\hat{n}}{\partial\hat{x}^2}+\frac{\partial}{\partial\hat{x}}(\hat{n}\hat{e}) \tag{10}$$

where the caret superscript indicates a dimensionless variable or parameter. The parameter $\hat{v}$ is the dimensionless group $\hat{v}=vq/k_BT$, where k_BT/q is the thermal voltage. The dimensionless charge conservation equation for holes is

$$\frac{\partial\hat{h}}{\partial\hat{t}}=\frac{\hat{m}}{\hat{v}}\frac{\partial^2\hat{h}}{\partial\hat{x}^2}-\hat{m}\frac{\partial}{\partial\hat{x}}(\hat{h}\hat{e}) \tag{11}$$

where $\hat{m}=\mu_h/\mu_p$ is the ratio of the hole mobility to the cation mobility. The dimensionless Poisson equation is

$$\hat{\epsilon}^2\hat{v}\frac{\partial\hat{e}}{\partial\hat{x}}=\frac{1}{2}(\hat{p}+\hat{h}-\hat{n}-1) \tag{12}$$

where $\hat{\epsilon}$ is the ratio of the Debye length $\lambda_d=\sqrt{\varepsilon k_BT/2q^2a}$ to the width of the film, defined as $\hat{\epsilon}=\lambda_d/l$. The Debye length characterizes the width of the screening layer adjacent to a charged surface, such as the polymer-electrolyte or polymer-cathode interfaces. In the device designed by Stavrinidou et al.,[18] $\hat{\epsilon}\approx10^{-9}$ based on a PEDOT:PSS dielectric constant of $\varepsilon_r=3.5$, $l=32$ mm, $T=300$ K, and $a=3\times10^{20}\text{cm}^{-3}$.[18] In the numerical solution to the full drift-diffusion equations, the dimensionless Debye length is taken to be $\hat{\epsilon}=0.001$. This value of $\hat{\epsilon}$ was selected because the experimental value is numerically intractable with the solvers used here. However, note that the larger value of $\hat{\epsilon}$ should not affect the dynamics as the majority of the film is electroneutral. The dimensionless boundary and initial conditions for cations are

$$\hat{p}(0,\hat{t})=1,\ \frac{\partial\hat{p}(1,\hat{t})}{\partial\hat{x}}=\hat{v}\hat{p}(1,\hat{t})\hat{e}(1,\hat{t})\ \text{and}\ \hat{p}(\hat{x},0)=0 \tag{13}$$

Similarly, the dimensionless boundary and initial conditions for anions are

$$\hat{n}(0,\hat{t})=1,\ \frac{\partial\hat{n}(1,\hat{t})}{\partial\hat{x}}=-\hat{v}\hat{n}(1,\hat{t})\hat{e}(1,\hat{t})\ \text{and}\ \hat{n}(\hat{x},0)=0 \tag{14}$$

The dimensionless boundary and initial conditions for holes are

$$\frac{\partial\hat{h}(0,\hat{t})}{\partial\hat{x}}=\hat{v}\hat{h}(0,\hat{t})\hat{e}(0,\hat{t}),\ \hat{h}(1,\hat{t})=1\ \text{and}\ \hat{h}(\hat{x},0)=1 \tag{15}$$

Finally, the dimensionless boundary conditions for the electric potential are

$$\hat{\phi}(0,\hat{t})=0\ \text{and}\ \hat{\phi}(1,\hat{t})=-1 \tag{16}$$

The dimensionless equations (10)–(12) and boundary conditions (13)–(16) are the basis for our analysis of moving

front dynamics in a planar MIEC device. In the following section, we consider a simplified description of front dynamics at large voltages, which is followed by numerical solution of the full equations in the results section.

Large Voltage Analysis: Similarity Solution

The governing equations (10)–(16) presented above can be simplified by considering the experimentally relevant case of a large voltage, a high hole-to-cation mobility ratio, and local electroneutrality. At large voltages $\hat{v} \gg 1$, the flux of anions from the electrolyte into the film can be neglected, as the strongly biased voltage prevents their entry. The smallness of the Debye length $\hat{\epsilon} \approx 10^{-9}$ in Stavrinidou et al.'s[18] experiments indicates that the charge density is confined to extremely thin regions immediately adjacent to the electrolyte- and electrode-polymer film interfaces, while the bulk of the film is electroneutral. When we assume electroneutrality and neglect the presence of anions in the film, Poisson's equation (12) is replaced by the algebraic constraint

$$\hat{p}+\hat{h}=1 \tag{17}$$

Lastly, a mobility ratio of $\hat{m} \sim 100$ is expected.[19] As the mobility ratio increases to infinity, the potential drop is confined to the cation-rich region behind the moving front, and the electric field in the hole-rich region approaches zero. Effectively, the resistance of the hole region is negligible in comparison to that of the cation region. Henceforth, we assume the limit $\hat{m} \to \infty$.

Under the above assumptions, the drift-diffusion equations (10)–(12) can be transformed from partial differential equations to ordinary differential equations via a similarity transformation. The similarity transformation asserts that the relevant length scale in the problem is the (unknown *aprioi*) invasion length δ, rather than the film width l. This is reasonable at the above conditions ($\hat{v} \gg 1$, $\hat{m} \gg 1$) as the voltage is effectively dropped across δ rather than l.

An expression for δ can be found via the following argument. Assuming that electromigration is the dominant transport mechanism for ions, the velocity of the front, $d\delta/dt \sim \mu_p e$. The field exists primarily in the cation-rich region, hence, $e \sim v/\delta$, giving $d\delta/dt \sim \mu_p v/\delta$ and thus $\delta \sim \sqrt{\mu_p v t}$. For ease of algebra, we multiply the right-hand side by $\sqrt{2}$ and define

$$\delta(t)=\sqrt{2\mu_p v t} \tag{18}$$

The invasion length δ is normalized by the film width l; and time by $l^2/\mu_p v$, the cation migration timescale. The dimensionless invasion length is

$$\hat{\delta}(\hat{t})=\sqrt{2\hat{t}} \tag{19}$$

This result is consistent with the invasion length given by the circuit model of Stavrinidou et al.[19] A similarity variable $\hat{\eta}$ is defined as

$$\hat{\eta}=\frac{\hat{x}}{\sqrt{2\hat{t}}} \tag{20}$$

To transform the governing equations, we first redefine the dependent variables in terms of the similarity variable, $\hat{\eta}$. The cation density is $\hat{p}(\hat{x},\hat{t})=\hat{P}(\hat{\eta})$, and the hole density is $\hat{h}(\hat{x},\hat{t})=\hat{H}(\hat{\eta})$. The electric field scales as the potential, $\hat{\phi}(\hat{x},\hat{t})$, divided by $\hat{\delta}$, as the bulk of the potential drop is confined to the cation-rich region of width $\hat{\delta}$. The electric field scaling is, therefore, $\hat{e}(\hat{x},\hat{t})=\hat{E}(\hat{\eta})/\hat{\delta}$.

The cation density at the electrode ($\hat{x}=1$) satisfies a no-flux condition (13). It is expected that the similarity solution should be valid at early times when the moving front is far from the electrode and unaffected by its presence; that is, the front effectively advances into a semiinfinite half-space. Hence, this no-flux condition is replaced by the requirement that the cation density is equal to zero far ahead of the front, $\hat{p}(\infty,\hat{t})=0$. This new boundary condition and the initial condition $\hat{p}(\hat{x},0)=0$ collapse into a single boundary condition as $\hat{\eta} \to \infty$. The two boundary conditions for the cation density are thus

$$\hat{P}(0)=1 \text{ and } \hat{P}(\infty) \to 0 \tag{21}$$

Assuming that the potential drop occurs in the cation-rich region and that the potential is constant in the hole-rich region, the electric field beyond the moving front is zero. In terms of the similarity variable, then

$$\hat{E}(\infty) \to 0 \tag{22}$$

The transformed cation conservation equation (10) is thus

$$\hat{\eta}\frac{d\hat{P}}{d\hat{\eta}}=-\frac{1}{\hat{v}}\frac{d^2\hat{P}}{d\hat{\eta}^2}+\frac{d}{d\hat{\eta}}(\hat{P}\hat{E}) \tag{23}$$

The tranformed hole equation (11) is

$$\frac{\hat{\eta}}{\hat{m}}\frac{d\hat{H}}{d\hat{\eta}}=-\frac{1}{\hat{v}}\frac{d^2\hat{H}}{d\hat{\eta}^2}+\frac{d}{d\hat{\eta}}(\hat{H}\hat{E}) \tag{24}$$

The similarity solution is only valid when the mobility ratio $\hat{m} \to \infty$, indicating that there is no potential drop across the hole-rich region. At this limit, the left-hand side of (24) is negligible in comparison to the right-hand side. Thus, the hole density satisfies the equation

$$0=-\frac{1}{\hat{v}}\frac{d^2\hat{H}}{d\hat{\eta}^2}+\frac{d}{d\hat{\eta}}(\hat{H}\hat{E}) \tag{25}$$

Equation 25 implies that the holes evolve in a quasisteady manner. As they are infinitely more mobile than the cations, they respond instantaneously to the slow cation front dynamics. The electroneutrality equation (17), $\hat{H}=1-\hat{P}$, is inserted into (25) to eliminate $\hat{H}$, yielding after rearrangement

$$-\frac{1}{\hat{v}}\frac{d^2\hat{P}}{d\hat{\eta}^2}+\frac{d}{d\hat{\eta}}(\hat{P}\hat{E})=\frac{d\hat{E}}{d\hat{\eta}} \tag{26}$$

The left-hand side of (26) is equal to the right-hand side of (23). Combining these two equations yields

$$\hat{\eta}\frac{d\hat{P}}{d\hat{\eta}}=\frac{d\hat{E}}{d\hat{\eta}} \tag{27}$$

Equations 23 and 27 and the boundary conditions (21) and (22) are solved simultaneously to give the cation density and electric field profiles. These equations are ordinary differential equations and thereby easier to solve numerically than the full partial differential drift-diffusion equations. Moreover, the similarity transformation yields considerable insight into the physics of the cation invasion process, revealing the self-similarity of the moving front dynamics.

Results

We solve the self-similar differential equations (23) and (27) with MATLAB'S bvp4c function, a collocation code for

Table 1. Summary of the Parameters Used in the Solution to the Full Drift-Diffusion Equations and the Similarity Solution in Comparison to the Dimensionless Experimental Parameters

	Full Drift-Diffusion	Similarity Solution	Experiments
Debye length, $\hat{\epsilon}$	10^{-3}	0	2×10^{-9}
Applied voltage, $\hat{v}$	40	40 and 76.92	76.92
Mobility ratio, $\hat{m}$	10^2	∞	10^2

The dimensional experimental parameters are as follows: $\lambda_d=2\times10^{-11}$ m, $v=2$ V, and $\mu_p=0.144\,\mathrm{mm}^2/\mathrm{Vs}$. The similarity solution is compared with both the full drift-diffusion equations and the experiments, so two applied voltages are listed.

boundary value problems.[34] The semiinfinite domain $\eta=[0,\infty)$ is truncated at a finite value η_f; the similarity equations are solved at progressively larger values of η_f to ensure convergence. Here, we present comparisons between the similarity solution and the solution to the full drift-diffusion equations (10)–(16), which are solved numerically by MATLAB'S pdepe function. The parameters used in comparing the similarity solution to the numerical solution of the full drift-diffusion equations and the experiments are summarized in Table 1.

Figure 3 compares the evolution of the ionic charge density and electric field across the film from the similarity solution and full drift-diffusion equations. The dimensionless voltage is $\hat{v}=40$, which corresponds to a voltage of 1.02 volts, an experimentally relevant voltage. In the solution to the full drift-diffusion equations, $\hat{\epsilon}=0.001$. Admittedly, this value of $\hat{\epsilon}$ is much larger than in experiments, where $\hat{\epsilon}\approx10^{-9}$; at smaller values of $\hat{\epsilon}$ sharp gradients in the ion profiles develop in the screening layers at the electrolyte-film and film-electrode interfaces that render the solution to the full drift-diffusion equations numerically intractable. This underscores the utility of the similarity solution, which is much easier to solve numerically yet evidently compares very well with the full drift-diffusion equations. To obtain converged solutions to the full drift at smaller values of $\hat{\epsilon}$, the pdepe solver could be replaced with more powerful numerical schemes. Another approach would be to combine numerical solution with singular perturbation analysis of the rapid variation in concentration and electric potential within the Debye (or boundary) layers. We selected the pdepe solver in MATLAB because it is simple to implement. The fact that the solution of the full drift-diffusion equations agrees well with the similarity solution validates our comparison of the similarity solution to the experimental results.

At early times, the electric field is extremely large (Figure 3a), because the potential drop is confined to the narrow region behind the moving front that has barely infiltrated the film. As the front progresses, the electric field weakens as the potential drops over a widening cation-rich region. This evolution is reflected in the ionic charge density profile, given in Figure 3b. Specifically, the cation front is sharp at early times, indicating the dominance of electromigration under the initially strong field. The front then broadens diffusively as it is driven to the electrode by the weakening field. The most significant deviation between the similarity solution and the full drift-diffusion equations occurs at the electrolyte-film interface ($x=0$), where the full drift-diffusion equations capture charge accumulation in the thin Debye layer (Figure 3b) and a spike in the electric field (Figure 3a). Recall, the similarity solution assumes electroneutrality and hence neglects the presence of the Debye layer. Nevertheless, the overall agreement between the similarity solution and the full numerical solution is excellent, which lends confidence to the assertion that invasion dynamics are self-similar.

To quantify the persistence of the $t^{1/2}$ scaling of the front location, we calculated the moving front location at each time step, defined as the x-position where the ionic charge density $\hat{p}-\hat{n}=0.5$. This plot is shown in Figure 4. At large voltages, the similarity solution prediction of the front location is accurate up until the point where the moving front reaches the electrode. This is a surprising result given that the similarity solution is formally valid only at early times, when the front is far from the electrode, $\delta \ll l$ (in dimensionless terms $\hat{x} \ll 1$). To explain this, recall that the

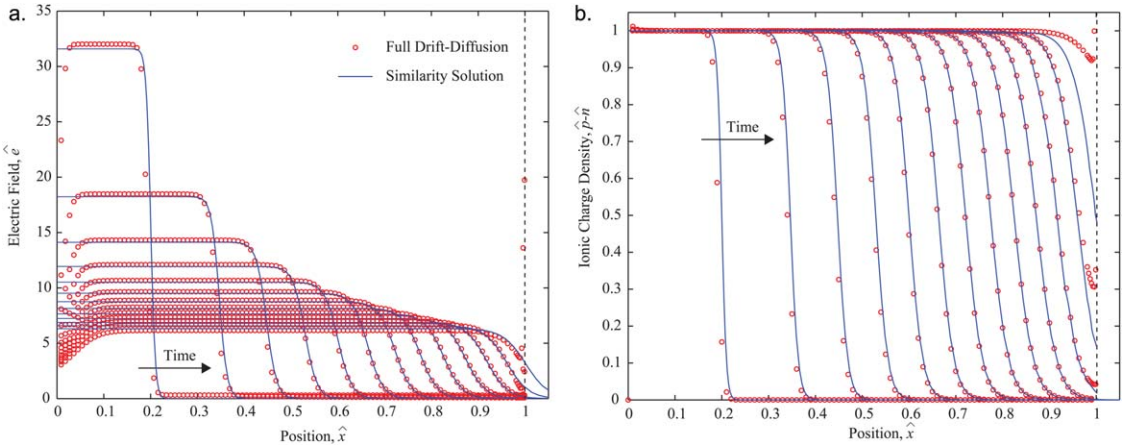

Figure 3. Comparison of the similarity solution (line) to the solution of the full drift-diffusion equations (circles) for (a) the electric field $\hat{e}$ and (b) the ionic charge density $\hat{p}-\hat{n}$.

Note that in the similarity solution $\hat{n}=0$, so that the ionic charge density is equal to the cation density $\hat{p}$. The dimensionless applied voltage is $\hat{v}=40$ which corresponds to a dimensional voltage of 1.02 volts, the mobility ratio $\hat{m}=100$, and the dimensionless Debye length is $\hat{\epsilon}=0.001$. The first curve from left to right is at $\hat{t}=0.02$, and each successive curve corresponds to a time increment of 0.04. After the front reaches the wall in (b), the charge accumulates in a Debye layer, leading to a spike in the electric field in (a). [Color figure can be viewed in the online issue, which is available at wileyonlinelibrary.com.]

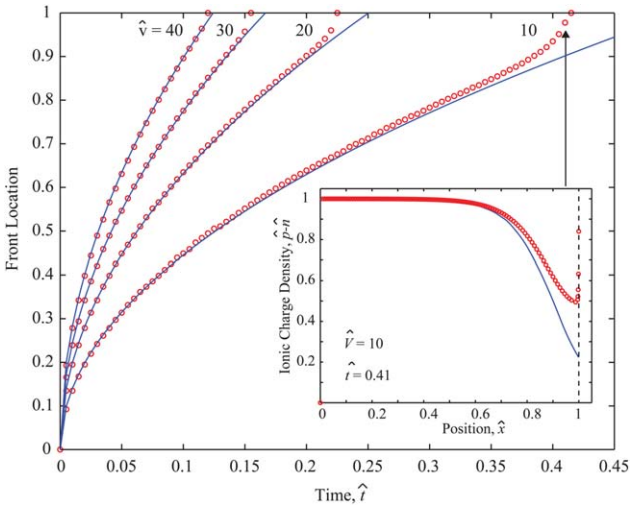

Figure 4. The time dependence of the location of the moving front (the position where $\hat{p}-\hat{n}=0.5$) from the similarity solution (19) for the dimensionless moving front location (solid line) is compared with the solution of the full drift-diffusion equations (circles) at various voltages, $\hat{v}=10, 20, 30, 40$.

Time $\hat{t}$ is dependent on voltage; here $\hat{t}$ is scaled by $\hat{v}=10$ Inset: the ionic charge density profile at $\hat{v}=10$ after the front reaches the electrode ($\hat{t}=0.41$). The full drift-diffusion equations capture the formation of a Debye layer, while the similarity solution does not. [Color figure can be viewed in the online issue, which is available at wileyonlinelibrary.com.]

position of the front advances under the applied voltage as $\delta \sim \sqrt{\mu_p v t}$. The thickness Δ of the front broadens diffusively as $\Delta \sim (t\mu_p k_B T/q)^{1/2}$, independent of the voltage. The ratio of the front thickness to front location is then $\Delta/\delta \sim (k_B T/vq)^{1/2}$, which decreases with increasing voltage as $v^{-1/2}$. Hence, at low voltages, the diffusive thickening of the front causes the ions at the leading edge of the front to reach the electrode well before the bulk of the front, as seen in the inset of Figure 4. Those leading ions then form a Debye layer at the electrode which causes the disparity between the front location predicted by the similarity solution and full solution. At larger voltages, the front does not have the opportunity to thicken before it reaches the electrode. Consequently, the bulk of the ions reach the electrode very shortly after the ions at the leading edge, thereby reducing the disparity between the full drift-diffusion solution and the similarity solution.

Stavrinidou et al.[18] measured the change in transmittance of an electrochromatic PEDOT:PSS polymer film during potassium invasion. Assuming that the transmittance is equal to the normalized cation density, in Figure 5, we digitized the transmittance data given in Figure 1c of Stavrinidou et al.[18] and compared it to the similarity solution. The applied voltage in the experiment is 2 volts, or $\hat{v}=76.92$, and the potassium mobility is $\mu_p=0.14\pm0.02\,\mathrm{mm^2/Vs}$, as calculated by Stavrinidou et al.[18] In the inset, Figure 5c, we fit the square of the front location with (19) and find that the data do not pass through the origin, indicating that there is a time lag between the time that the voltage is applied and the invasion of the cations. To account for this, we modified (19) to include a time lag term t_{lag}. We fit the modified expression, $\delta^2=2\mu_p v(t-t_{lag})$, to the data and estimated the time lag to be $t_{lag}=2.73\,\mathrm{s}$. The value of t_{lag} does not affect the similarity solution, aside from a shift in the cation density profiles with respect to time.

These experiments are conducted at an early time, when the moving front is between 0 and 8 mm from the electrolyte in a 32-mm thick film. In Figure 5a, we plot our similarity solution for the cation density against the transmittance data and find that while the expression for δ (18) accurately predicts the location of the moving front, the similarity solution for the cation density profile is much steeper than that of the experiments. This begs the question: do the experiments exhibit self-similar front dynamics? To answer this, in Figure 5b, we transformed the experimental transmittance

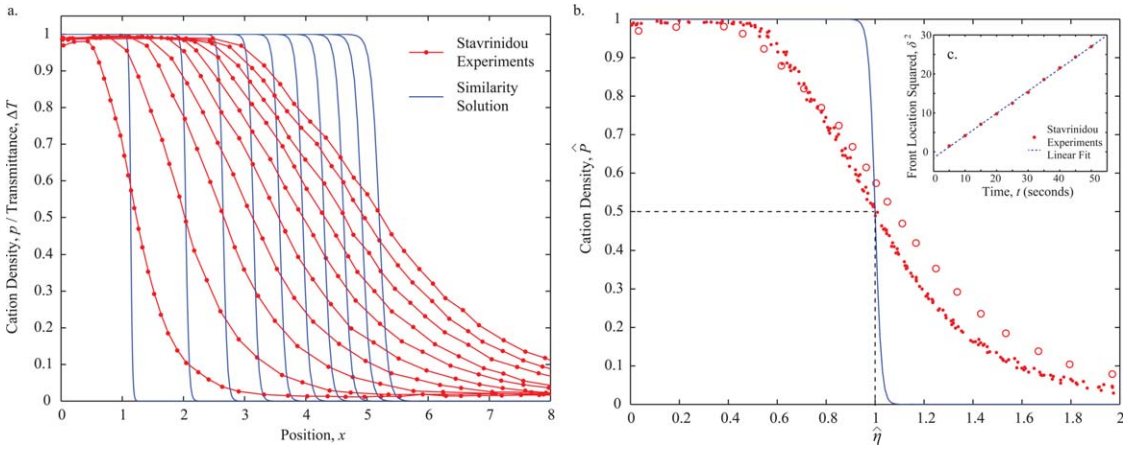

Figure 5. (a) Comparison between transmittance data by Stavrinidou et al.[18] (symbols joined by line) and the similarity solution for the cation density (line) at an applied voltage of 2 V ($v=76.92$), $\mu_p=0.14\,\mathrm{mm^2/Vs}$, and a time lag of $t_{lag}=2.73\,\mathrm{s}$. The transmittance profiles are shown at 5 s increments. (b) The x-position of the experimental data (red dots) is transformed to the similarity variable η. The experimental data collapse to a single curve, indicating self-similarity, with the exception of the data from the first time step (red open circle). (c) The square of the front location where $p=0.5$ (circles) is plotted against time and fitted (solid line) to determine the mobility μ_p and the time lag t_{lag}.

[Color figure can be viewed in the online issue, which is available at wileyonlinelibrary.com.]

data from $\Delta T(x,t)$ to $\hat{\Delta}T(\hat{\eta})$ by dividing the x-position by δ, given by (18). After the transformation, the transmittance data collapse to a single curve, with the exception of the transmittance at the first time step, indicating that the invasion process is self-similar, and that the front scaling is in fact given by (18). However, qualitative differences in the spatial profiles are seen in Figure 5, suggesting that additional physical effects are at play in the experiments.

We investigate this discrepancy further by relaxing several assumptions. First, we assumed that the cation and hole mobilities are constant, despite the large variations in the electric field (Figure 3a). To relax this assumption, we endow the mobility with a simple power-law dependence on the electric field, $\mu_p=\mu_{p0}(e/e_0)^s$, where s is the power law index, $e_0=k_BT/ql$, and μ_{p0} is the mobility at e_0. We look for similarity solutions of the drift-diffusion equations with the generalized similarity variable $\hat{\eta}=(\hat{x}+\hat{B}\hat{t}^{\alpha})/\hat{A}\hat{t}^{\beta}$, where $\hat{B}\hat{t}^{\alpha}$ (B is a constant) controls the advancement of the front and $\hat{A}\hat{t}^{\beta}$ (A is a constant) dictates the thickening of the front.[31] Our hope is to find similarity solutions with $\alpha=1/2$ and $\beta > 1/2$ to capture the broader (or thicker) density profile seen in the experiments as compared with our existing similarity solution with a field-independent mobility ($s=0$). It can be shown that $\alpha=\beta=1/(s+2)$ is required for a similarity solution to exist, revealing that the drift-diffusion equations exhibit a family of self-similar solutions for a power-law-dependent mobility. Interestingly, when $s=-1$ (the mobility increases with decreasing electric field) the front advances and thickens linearly in time. However, the experiments clearly show that the front advances as $t^{1/2}$, consistent with $\alpha=1/2$. The slope of the experimental transmittance data points within 0.2η of the midpoint in Figure 5 is a constant, calculated to be approximately -1. Thus, the slope of the front dp/dx scales as $t^{-1/2}$. The thickness of the moving front is inversely proportional to the slope, so it follows that the thickness scales with the $t^{1/2}$ and $\beta=1/2$. This implies that the simple power-law-dependent mobility cannot yield a similarity solution with a front that advances as $t^{1/2}$ while thickening at a greater rate.

A second issue may be voltage losses in the electrolyte and at the electrolyte-film and film-electrode interfaces, leading to a reduced driving voltage across the film. To test this hypothesis, we fit the similarity solution to the experimental data[18] with two adjustable parameters: the applied voltage v and cation mobility μ_p. The best fit between the similarity solution and the experimental data requires an order of magnitude decrease in the applied voltage and an order of magnitude increase in the cation mobility from the reported values,[18] which does not seem plausible.

Another effect involving the electric potential is the possibility of a Donnan potential difference between the electrolyte and the negatively charged polymer film.[35] The existence of such a potential difference would cause an increase in cation concentration at the electrolyte-polymer interface relative to its value in the electrolyte reservoir. We have examined whether such an increase in ion concentration alters the shape of the moving ion front as follows. The ratio of the cation concentration at the interface to the hole concentration was varied from 1:1 to 1.5:1 and 0.5:1 in our numerical solution, by adjusting the ion boundary conditions (13) and (14). Deviations from the 1:1 ratio hitherto assumed result in a change in the moving front location, but there is no significant change in the slope of the cation density profiles. It is, therefore, unlikely that a local increase in ion concentration at the electrolyte-polymer film interface due to a Donnan potential difference is responsible for the mismatch in front shape between theory and experiment.

Third, our assumption of 1-D ion transport neglects the possible existence of screening layers due to surface charges at the interfaces of the film with the glass substrate and the Su-8 ion barrier. These layers could provide another path for (surface) conductivity of the cation front. A more sophisticated analysis could be performed by depth-averaging the drift-diffusion equations to arrive at effective 1-D transport equations that account for these screening layers.[28] Another reason for the discrepancy may be a delay before the applied field is switched on, allowing for cations and anions to diffuse into the film and altering the initial condition. We tested this idea and found that while the front location increases, the shape of the cation density profile does not change significantly. Finally, there is the possibility that the change in transmittance is not a precise proxy for the cation density profile. We hope that the present work will inspire additional experimental and modeling efforts. For example, an alternative method for measuring the cation density across the film would provide verification of the transmittance as an accurate measure of cation density. Experiments reporting invasion dynamics across the entire film as opposed to the initial stages would enable a verification of the persistence of the $t^{1/2}$ scaling provided by our analysis.

Conclusion

Motivated by the recent experiments of Stavrinidou et al.,[18] we have analyzed the moving front dynamics of cations invading a MIEC polymer film. Our work demonstrates that the invasion process is self-similar at the large driving voltages used in the experiments, and confirms that the front location advances with a square-root-of-time scaling, $t^{1/2}$. The thickness of the cation front also grows as $t^{1/2}$. Remarkably, at larges voltages, $\hat{v} \gg 1$, the similarity solution is in excellent agreement with the numerical solution of the full drift-diffusion equations until the point that the front reaches the end of the film. The agreement between solutions of the full drift-diffusion equations and the similarity solution validates the reliability of the numerical methods. We compared our similarity solution to the aforementioned experiments: although both display self-similar evolution of the ion front with a $t^{1/2}$ advancement, the experimental ion density profile (which we assumed to be equal to the reported transmittance data) is considerably broader than we predict. We hope the discrepancy between theory and experiment will motivate further work on this subject.

The present problem is similar to that of ion concentration polarization shocks in microchannel-nanochannel systems under constant voltage.[30] A cation-selective nanochannel acts a junction between two microchannels. The application of a fixed voltage results in a depleted ion concentration polarization zone in one microchannel and an enriched zone in the other. Under certain conditions, the zones can propagate as shocks; the depletion shock advances with a $t^{1/2}$ scaling, and its thickness grows as $t^{1/2}$. This depletion zone is equivalent to the cation front in the present problem: namely, both are low-conductivity regions displacing a region of higher conductivity. In our problem, the high-conductivity region is the hole-rich region of the film, whereas in the concentration polarization problem, it is the electroneutral electrolyte ahead of the depletion shock. Importantly, in both problems the majority of the potential drop occurs across the

low-conductivity region behind the advancing front. At constant current, a concentration polarization depletion shock propagates linearly in time[28,30]; hence, it is expected that cation front invasion would also advance linearly with t if the device of Stavrinidou et al.[18] were operated at constant current conditions. This mode of operation may also provide another method to measure the ion mobility in MIEC films.

Another analogy to cation invasion is capillary filling, in which a viscous liquid is drawn into a capillary by a pressure difference, displacing the air in the tube. The location of the advancing liquid front (or meniscus) again increases with a square-root-of-time scaling, a result referred to as Washburn's law.[36] Once more, this is a situation where a low-conductivity region (the liquid) invades a high-conductivity region (the inviscid air). The pressure difference across the capillary plays the role of the driving voltage, and the liquid and air regions are analogous to the cation and hole regions, respectively. It is well known that the displacement of a low viscosity fluid by a high viscosity fluid is stable, whereas the opposite scenario is susceptible to viscous fingering (Saffman–Taylor) instability.[37] Therefore, the cation invasion front should also be stable and remain uniform against perturbations transverse to the propagation direction, which could be caused by, for example, variation in the MIEC film morphology. On a related note, Mani and Bazant[31] demonstrated that depletion concentration polarization (or deionization) shocks at constant current evolve via the process of inverse Laplacian growth, which also yields stable and uniform fronts in disordered microstructures. We leave the interesting subject of front invasion dynamics in inhomogenous MIEC films to future work.

Acknowledgment

S. E. F. acknowledges support by the National Science Foundation Graduate Research Fellowship under Grant No. 0946825.

Literature Cited

1. Riess I. Mixed ionic–electronic conductorsmaterial properties and applications. *Solid State Ionics*. 2003;157(1):1–17.
2. Crone B, Dodabalapur A, Gelperin A, Torsi L, Katz HE, Lovinger AJ, Bao Z. Electronic sensing of vapors with organic transistors. *Appl Phys Lett*. 2001;78(15):2229–2231.
3. Chang JB, Liu V, Vivek S, Sivula K, Luscombe C, Murphy A, Liu J, Fréchet JMJ. Printable polythiophene gas sensor array for low-cost electronic noses. *J Appl Phys*. 2006;100(1):014506.
4. Pei Q, Yu G, Zhang C, Yang Y, Heeger AJ. Polymer light-emitting electrochemical cells. *Science*. 1995;269(5227):1086–1088.
5. van Reenen S, Matyba P, Dzwilewski A, Janssen RAJ, Edman L, Kemerink M. A unifying model for the operation of light-emitting electrochemical cells. *J Am Chem Soc*. 2010;132:13776–13781.
6. Schön JH, Dodabalapur A, Bao Z, Kloc C, Schenker O, Batlogg B. Gate-induced superconductivity in a solution-processed organic polymer film. *Nature*. 2001;410(6825):189–192.
7. Frackowiak E, Khomenko V, Jurewicz K, Lota K, Beguin F. Supercapacitors based on conducting polymers/nanotubes composites. *J Power Sources*. 2006;153(2):413–418.
8. Koezuka H, Tsumura A, Ando T. Field-effect transistor with polythiophene thin film. *Synth Met*. 1987;18(1):699–704.
9. Cramer T, Campana A, Leonardi F, Casalini S, Kyndiah A, Murgia M, Biscarini F. Water-gated organic field effect transistors–opportunities for biochemical sensing and extracellular signal transduction. *J Mater Chem B*. 2013;1(31):3728–3741.
10. Leger JM. Organic electronics: the ions have it. *Adv Mater*. 2008; 20(4):837–841.
11. White HS, Kittlesen GP, Wrighton M. Chemical derivatization of an array of three gold microelectrodes with polypyrrole: fabrication of a molecule-based transistor. *J Am Chem Soc*. 1984;106(18):5375–5377.
12. Bernards DA, Malliaras GG. Steady-state and transient behavior of organic electrochemical transistors. *Adv Funct Mater*. 2007;17(17): 3538–3544.
13. Bernards DA, Macaya DJ, Nikolou M, DeFranco JA, Takamatsu S, Malliaras GG. Enzymatic sensing with organic electrochemical transistors. *J Mater Chem*. 2007;18(1):116–120.
14. Tarabella G, Nanda G, Villani M, Coppedè N, Mosca R, Malliaras GG, Santato C, Iannotta S, Cicoira F. Organic electrochemical transistors monitoring micelle formation. *Chem Sci*. 2012;3(12):3432–3435.
15. Berggren M, Richter-Dahlfors A. Organic bioelectronics. *Adv Mater*. 2007;19(20):3201–3213.
16. Campbell IH, Smith DL, Neef CJ, Ferraris JP. Consistent time-of-flight mobility measurements and polymer light-emitting diode current–voltage characteristics. *Appl Phys Lett*. 1999;74(19):2809–2811.
17. Borsenberger PM, Weiss DS. Organic Photoreceptors for Xerography. New York: Marcel Dekker, 1998.
18. Stavrinidou E, Leleux P, Rajaona H, Khodagholy D, Rivnay J, Lindau M, Sanaur S, Malliaras GG. Direct measurement of ion mobility in a conducting polymer. *Adv Mater*. 2013;25:4488–4493.
19. Stavrinidou E, Leleux P, Rajaona H, Fiocchi M, Sanaur S, Malliaras GG. A simple model for ion injection and transport in conducting polymers. *J Appl Phys*. 2013;113(24):244501–244501.
20. Aoki K, Aramoto T, Hoshino Y. Photographic measurements of propagation speeds of the conducting zone in polyaniline films during electrochemical switching. *J Electroanal Chem*. 1992;340(1): 127–135.
21. Carlberg JC, Inganäs O. Fast optical spectroscopy of the electrochemical doping of poly (3, 4-ethylenedioxythiophene). *J Electrochem Soc*. 1998;145(11):3810–3814.
22. Lacroix JC, Fraoua K, Lacaze PC. Moving front phenomena in the switching of conductive polymers. *J Electroanal Chem*. 1998;444(1): 83–93.
23. Johansson T, Persson NK, Inganäs O. Moving redox fronts in conjugated polymers studies from lateral electrochemistry in polythiophenes. *J Electrochem Soc*. 2004;151(4):E119–E124.
24. Chen Z, Ghosal S. The nonlinear electromigration of analytes into confined spaces. *Proc R Soc A: Math Phys Eng Sci*. 2012;468(2146): 3139–3152.
25. Saville DA, Palusinski OA. Theory of electrophoretic separations. Part I: formulation of a mathematical model. *AIChE J*. 1986;32(2): 207–214.
26. Fife PC, Palusinski OA, Su Y. Electrophoretic traveling waves. *Trans Am Math Soc*. 1988;310(2):759–780.
27. Ghosal S, Chen Z. Nonlinear waves in capillary electrophoresis. *Bull Math Biol*. 2010;72(8):2047–2066.
28. Mani A, Zangle TA, Santiago JG. On the propagation of concentration polarization from microchannel-nanochannel interfaces Part I: analytical model and characteristic analysis. *Langmuir*. 2009;25(6): 3898–3908.
29. Zangle TA, Mani A, Santiago JG. On the propagation of concentration polarization from microchannel-nanochannel interfaces Part II: numerical and experimental study. *Langmuir*. 2009;25(6):3909–3916.
30. Zangle TA, Mani A, Santiago JG. Effects of constant voltage on time evolution of propagating concentration polarization. *Anal Chem*. 2010;82(8):3114–3117.
31. Mani A, Bazant MZ. Deionization shocks in microstructures. *Phys Rev E*. 2011;84(6):061504.
32. Pai DM. Transient photoconductivity in poly(W-vinylcarbazole). *J Chem Phys*. 1970;52(5):2285–2291.
33. Blom PWM, De Jong MJM, Van Munster MG. Electric-field and temperature dependence of the hole mobility in poly (p-phenylene vinylene). *Phys Rev B*. 1997;55(2):R656.
34. Shampine LF, Gladwell I, Thompson S. Solving ODEs with MATLAB. Cambridge: Cambridge University Press, 2003.
35. Davies JT, Rideal EK. *Interfacial Phenomena*. New York: Academic Press, 1961.
36. Washburn EW. The dynamics of capillary flow. *Phys Rev*. 1921; 17(3):273.
37. Saffman PG, Taylor G. The penetration of a fluid into a porous medium or Hele–Shaw cell containing a more viscous liquid. *Proc R Soc London A Math Phys Sci*. 1958;245(1242):312–329.

Manuscript received July 22, 2014, and revision received Jan. 12, 2015.